Can *et al. Molecular Cancer* (2025) 24:172
https://doi.org/10.1186/s12943-025-02371-1

Molecular Cancer

RESEARCH Open Access

Differential susceptibility and role for senescence in CART cells based on costimulatory domains

Ismail Can[1,2], Elizabeth L. Siegler[1,2], Olivia L. Sirpilla[1,3], Claudia Manriquez-Roman[1,4], Kun Yun[1,3], Carli M. Stewart[1,3], Jennifer M. Feigin[1,3], Makena L. Rodriguez[1,2], Omar L. Gutierrez-Ruiz[1,2], Ekene J. Ogbodo[1,2], Truc N. Huynh[1,2], Brooke L. Kimball[1,2], Long K. Mai[1,2], Mehrdad Hefazi[1,2], Lionel Kankeu Fonkoua[1,5], Hong Xia[1,2], Imene Hamaidi[7], Berke Alkan[6], Fatih Sezer[6], H. Atakan Ekiz[6], R. Leo Sakemura[1,2] and Saad S. Kenderian[1,2,3,4*]

Abstract

Despite the success of chimeric antigen receptor T (CART) cell therapy in hematological malignancies, durable remissions remain low. Here, we report CART senescence as a potential resistance mechanism in 41BB-costimulated CART cell therapy. To mimic cancer relapse, we utilized an in vitro model with repeated CART cell activation cycles followed by rest periods. Using CD19-targeted CART cells with costimulation via 4-1BB-CD3ζ (BBζ) or CD28-CD3ζ (28ζ), we showed that CART cells undergo functional, phenotypical, and transcriptomic changes of senescence, which is more prominent in BBζ. We then utilized two additional independent strategies to induce senescence through MYC activation and irradiation. Induction of senescence impaired BBζ activity but improved 28ζ activity in preclinical studies. These findings were supported by analyses of independent patient data sets; senescence signatures in CART cell products were associated with non-response to BBζ but with improved clinical outcomes in 28ζ treatment. In summary, our study identifies senescence as a potential mechanism of failure predominantly in 41BB-costimulated CART cells.

Significance

We identified senescence as a cause of failure in CART cell therapy, predominantly in 4-1BB-costimulated CART cells.

Keywords Chimeric antigen receptor T cell therapy, Senescence, Exhaustion, MYC, Immunotherapy

*Correspondence:
Saad S. Kenderian
kenderian.saad@mayo.edu
[1]T Cell Engineering, Mayo Clinic, Rochester, MN, USA
[2]Division of Hematology, Mayo Clinic, 200 First Street S.W, Rochester, MN 55905, USA
[3]Mayo Clinic Graduate School of Biomedical Sciences, Rochester, MN, USA
[4]Center for Regenerative Biotherapeutics, Mayo Clinic, Rochester, MN, USA
[5]Department of Oncology, Mayo Clinic, Rochester, MN, USA
[6]Department of Molecular Biology and Genetics, Izmir Institute of Technology, Izmir, Türkiye
[7]Cancer Biology, Mayo Clinic, Jacksonville, FL, USA

Introduction

Engineered T cells expressing chimeric antigen receptors (CART) have emerged as a novel and potentially curative immunotherapy in a subset of patients with relapsed/refractory hematological malignancies [1, 2]. Despite high initial responses in the clinic, most patients relapse within the first 1–2 years post-therapy [3]. Baseline T cell defects, inhibition by the tumor and its microenvironment, and suboptimal CART cell expansion and persistence have been identified as critical factors involved in CART cell failure [4–12].

Exhaustion is a state of dysfunction characterized by decreased T cell effector functions and upregulation of inhibitory receptors and pathways [13–15]. Exhaustion in CART cells has been studied extensively and demonstrated to be partly due to chronic CAR stimulation [10, 12, 16, 17]. Persistent T cell activation can induce exhaustion or senescence, both of which can prevent optimal T cell effector functions due to different underlying mechanisms [18–22]. Senescing cells enter a terminal state in which the cell cycle is irreversibly arrested, gain resistance to apoptosis, and develop a proinflammatory senescence-associated secretory phenotype (SASP) that causes chronic inflammation [23, 24]. Accumulation of senescence is associated with impaired tissue function, and selective removal of senescent cells has been shown to improve tissue integrity [23, 24]. Several independent studies have demonstrated alterations in genes involved in the development of senescence based on single cell sequencing analysis of CART cells, but it remains unknown if CART cells acquire a senescent phenotype and its potential impact on CART cell functions [25, 26].

We therefore assessed the development of senescence in CART cells across two CAR constructs similar to FDA-approved CD19-directed CART (CART19) products: CART19-41BBζ (BBζ) and CART19-CD28ζ (28ζ). The main difference between BBζ and 28ζ therapies is the costimulatory domain, which has been demonstrated to dictate CART cell functional phenotype and fate [19, 27–29]. Previous reports have suggested that 28ζ results in more pronounced T cell activation with exhaustion phenotype compared to BBζ, which has been characterized as having a milder but longer-lasting activation [25–27]. Here, we report the development of CART senescence as a mechanism of CART resistance and discovered costimulatory domain-specific senescence responses in both preclinical models and in clinical correlative data [25, 26].

Methods

Cell lines

The mantle cell lymphoma cell line JeKo-1 was purchased from ATCC (Manassas, VA, USA) and cultured in R20 medium, which contained RPMI 1640 (cat# 21870092, Gibco, Gaithersburg, MD, USA), 20% fetal bovine serum (cat# 250517, FBS, Sigma, St. Louis, MO, USA), and 1% penicillin-streptomycin-glutamine (PSG) (cat# 221675, Gibco). JeKo-1 was lentivirally transduced with luciferase-ZsGreen (pBMN (CMV-copGFP-Luc2-Puro), cat# 80389, Addgene, Cambridge, MA, USA) and sorted to 100% purity.

CART cell generation

CART cells were generated as previously described [8–10, 12, 30]. In summary, second-generation CAR constructs were synthesized de novo (Integrated DNA Technologies, Coralville, IA, USA) containing an anti-CD19 single chain variable fragment (clone FMC63) and either CD28-CD3ζ or 41BB-CD3ζ signaling domains in a third-generation lentiviral backbone. Lentiviral particles were generated through transfection of plasmids into HEK-293T cells (ATCC) using Lipofectamine 3000 (cat# L3000075, Invitrogen, Carlsbad, CA, USA). T cells were isolated from de-identified healthy donors on Day 0 (D0) using EasySep Human T Cell Isolation Kits (cat# 17951, STEMCELL Technologies, Vancouver, BC, Canada) and stimulated with CD3/CD28 Dynabeads (cat# 40203D, LifeTechnologies, Oslo, Norway) at a 3:1 beads-to-cell ratio. On Day 1, T cells were lentivirally transduced with the CAR constructs at a multiplicity of infection of 3. T cells were cultured in T cell medium containing X-Vivo 15 (cat# 123696, Lonza, Walkersville, MD, USA), 10% human serum albumin (cat# 12667-50ML-M, Corning, NY, USA), and 1% PSG (cat# 221675, Gibco). Beads were removed and CAR expression was assessed on Day 6. CART cells were used in the repeated activation cycle model beginning on Day 8. CAR expression was detected with anti-FMC63 (cat# FM3-AY54P1, ACROBiosystems, Newark, DE, USA).

In vitro model for CART cell failure

After generating untransduced control T cells (UTD), CART19-41BB-CD3ζ (BBζ), and CART19-CD28-CD3ζ (28ζ) cells through the eight-day protocol described above, T cells or Day 8 CART cells (UTD D8, BBζ D8, and 28ζ D8) were co-cultured with JeKo-1 cells that had been irradiated at 120 Gy (JeKo-1 IR) at a 1:1 effector-to-target ratio. A second round of 1:1 JeKo-1 IR was added to the co-culture after three days. The media was replaced with fresh media two days later, and CART cells were rested for two additional days before concluding the activation cycle and performing functional assays. As such, CART cells after one activation cycle were referred to as BBζ D15, and 28ζ D15.

T cell functional assays

CART cell proliferation and cytotoxicity assays were performed as previously described [9, 12, 30]. In summary, for killing assays, effector cells were cocultured

with luciferase$^+$ JeKo-1 cells at various ratios. Target killing was assessed at the indicated timepoints by adding 1 µL of 30 µg/mL D-luciferin (cat# LUCK-1G, Gold Biotechnology, St. Louis, MO, USA) per 100 µL media to the cocultures and performing bioluminescence imaging (BLI) (Promega GloMax Explorer, Madison, WI, USA) to measure the remaining live cells. For proliferation assays, effector cells and JeKo-1 cells were cocultured at a 1:1 ratio. After three days, absolute counts of CD3$^+$ cells were assessed via flow cytometry using anti-human CD3 (cat# 344818, BioLegend, San Diego, CA, USA) and LIVE/DEAD™ Fixable Aqua Dead Cell Stain Kit (cat# L34966, Invitrogen).

In vivo experiments

6- to 8-weeks old NOD-SCID-IL2rγ$^{-/-}$ (NSG) mice were purchased from Jackson Laboratories and were cared for at the Department of Comparative Medicine at the Mayo Clinic under an approved Institutional Animal Care and Use Committee protocol (A00001767-16-R22). Mice were intravenously engrafted with luciferase$^+$ 1×10^6 JeKo-1 cells, and tumor burden was serially assessed via BLI with a Xenogen IVIS-200 Spectrum camera (PerkinElmer, Hopkinton, MA, USA) as previously described [9, 12]. When tumor burden reached ~10^8 photons/second, mice were randomized to treatment with 1-1.5 $\times 10^6$ effector cells through tail vein injection as indicated in each experiment. Mice were monitored for tumor burden and overall survival.

CART cell in vivo expansion and cytokine analysis

In vivo cytokine profile and CART cell expansion were assessed by peripheral blood sampling. To determine CART cell counts, ~70µL of peripheral blood was collected from the tail vein and lysed of red blood cells with FACS™ Lysing Solution (cat# 349202, BD Biosciences, San Diego, CA, USA). Antibody staining was performed with anti-human CD3, anti-human CD45 (cat# 304032, BioLegend), anti-mouse CD45 (cat# 103116, BioLegend) and anti-human CD20 (cat# 980208, BioLegend). Flow cytometry was then performed to determine the absolute CD3$^+$ T cell count [12].

Cytokine concentration in the serum of mice was determined with MILLIPLEX MAP Human High Sensitivity T Cell Panel Premixed 13-plex (cat# HSTCMAG28P-MX13BK, Millipore Sigma, Ontario, Canada) according to the manufacturer's instructions. Analysis was completed with Belysa software after running the samples on a Luminex 200 (Millipore Sigma).

Intracellular staining

p21 Waf1/Cip1 (cat# CST 8865) and p53 (cat# CST 5429) antibodies were purchased from Cell Signaling Technology (CST) (Danvers, MA, USA). The cells were stained according to the manufacturer's recommendations. In summary, the cells were washed with PBS and fixed with 4% formaldehyde for 15 min at room temperature. Fixed cells were permeabilized with 90% methanol for 10 min on ice. The cells were stained with the antibodies for 1 h at room temperature for flow analysis. All measurements were performed in technical triplicates. Fluorescence minus one (FMO) was used as a negative control to provide the positive and negative gates.

EdU assay

UTD and CART cells were co-cultured with JeKo-1 IR at a 1:1 ratio in the presence of 2 µM EdU for 24 h and stained according to the manufacturer's protocol for Click-iT™ Plus EdU Alexa Fluor™ 647 Flow Cytometry Assay Kit from Life Technologies (cat# C10635). All measurements were performed in technical triplicates. Cells without EdU served as a negative control to gate the positive and negative EdU populations.

RNA isolation, rnaseq, and qPCR

Cells used for RNA isolation were cultured in serum-free media for 24 hours before being flash frozen and stored at -80°C until RNA isolation. RNA was isolated from ~1×10^7 cells in one batch with RNeasy Plus Mini Kit (cat# 74134, Qiagen, Hilden, Germany) according to the manufacturer's protocol. RNA quality was initially assessed using Qubit fluorometry (Invitrogen, Carlsbad, CA) and the Agilent Fragment Analyzer (Santa Clara, CA, USA). cDNA libraries were prepared using 100 ng of total RNA according to the manufacturer's instructions for the QuantSeq 3' mRNA-Seq Library Kit (Lexogen, Greenland, NH, USA). The concentration and size distribution of the completed libraries were determined using an Agilent TapeStation DNA 1000 chip (Santa Clara, CA, USA) and Qubit fluorometry (Invitrogen). Libraries were sequenced following Illumina's standard protocol for the NovaSeq 6000 (San Diego, CA, USA). The flow cell was sequenced as 100 bp single end reads using the NovaSeq SP sequencing kit and NovaSeq Control Software v1.7.5. Base-calling was performed using Illumina's RTA version 3.4.4.

cDNA for qPCR was produced with iScript Advanced cDNA Kit for real-time quantitative polymerase chain reaction (RT-qPCR) (cat# 1725038, Bio-Rad, Hercules, CA, USA) according to the manufacturer's suggestions. RT-qPCR was performed according to manufacturer's instructions with RT-qPCR SsoAdvanced Universal SYBR Green Supermix (cat# S7563, Bio-Rad).

Primers used for qPCR included TBP [31] (F: GCCAG CTTCGGAGAGTTCTGGGATT, R: CGGGCACGAAG TGCAATGGTCTTTA), p21 [31] (F: GCCATTAGCGC ATCACAGT, R: ACCGAGGCACTCAGAGGAG), p53 [31] (F: GAGGTTGGCTCTGACTGTACC, TCCGTCC

CAGTAGATTACCAC), MMP12 [31] (F: CTGAGGAC ATAGCAAATATGCAATAAA R: TGGTTTGGTTGTT AGAAATGGTGTA), MYC [32] (F: CCTACCCTCTCAA CGACAGC, R: CTCTGACCTTTTGCCAGGAG), uPAR [33] (F: CGAGGTTGTGTGTGGGTTA, R: GGCACTG TTCTTCAGGGCT) and PIM1 [34] (F: CGACATCAAG GACGAAAACATC, R: ACTC-TGGAGGGCTATACAC TC).

RNA-seq analysis

We utilized RNA-seq analysis to compare untransduced control T cell (UTD), BBζ D8 and D15, and 28ζ D8 and D15 ($n = 3$ per time point). Differentially expressed genes in UTD versus BBζ D8, D15 and 28ζ D8, D15 was analyzed using the "limma" (v3.58.1) R package after removing lowly expressed genes and voom transformation. Expression of SenMayo genes were visualized in heatmaps after scaling each gene and hierarchical clustering where distance metric was set to "correlation" and the clustering method was set to "complete" using "pheatmap" (v1.0.12) R package. Principal component analysis (PCA) was performed using the voom-normalized gene expression matrix via the "factoextra" R package (v1.0.7). The entire set of genes were used for this analysis and individual samples are visualized along the first two principal component axes. Lastly, we performed GSEA between select pairs of samples where the genome-wide log fold-change values were provided as a pre-ranked input to the fgsea algorithm (v1.28.0).

Analysis of scrnaseq data

scRNAseq data of patients with B-cell lymphoma treated with CART19 were downloaded from the GEO database (GSE197268) (previously reported in Haradhvala et al. (2022)) [25]. This data set consists of time-course analyses of PBMCs before and during treatment with axicabtagene ciloleucel (axi-cel, containing CD28 signaling domain) or tisagenlecleucel (tisa-cel, containing 4-1BB signaling domain). Raw barcode-feature matrices were processed using Seurat R package (v5.0.2) and low-quality cells containing < 200 or > 6000 mapped features and > 10% mitochondrial transcripts were removed from the analyses. Gene expression data were normalized using cpm method of Seurat and data were log2-transformed subsequently. 28 out of 32 patients with scRNAseq data on day 0 (infusion timepoint) and day 7 (on-treatment timepoint) were selected for further analysis. Out of these 28 patients, 15 patients were treated with axi-cel (9 with complete response [Axi_R], 6 with progressive disease [Axi_NR]) and 13 patients were treated with tisa-cel (5 with complete response [Tisa_R], 9 patients with progressive disease [Tisa_NR]). For gene set enrichment analyses (GSEA), single-cell data were converted to pseudobulk data by first "gating" cells based on CAR expression (non-zero counts of the annotated Yescarta and Kymriah transcripts) and calculating an average gene expression value for each gene. Pseudobulk data were aggregated across patients and GSEA was performed using fgsea R package (v1.28.0) following ranking genes based on their signal-to-noise ratio [35]. We also performed survival analysis using pseudobulk data from this cohort. To that end, we extracted progression-free survival duration for each patient by matching the FDG-PET scan timepoint and the classification of response at the time of the scan. We performed survival analysis using the "survival" (v3.5-8) and "survminer" (v0.4.9) R packages after categorizing the patients as high or low at the median value of the averaged senMayo gene set.

Western blot

Western blot was performed as described previously [36]. CART cell pellets were washed once with ice cold PBS. Then, the cell pellet was resuspended for 15 min on ice with cold cell lysis buffer (cat# R0278, RIPA buffer, Thermo Fisher, Waltham, MA, USA) with freshly added protease and phosphatase inhibitors (Halt™ Protease and Phosphatase Inhibitor Cocktail, Thermo Fisher, Waltham, MA, USA). Protein concentration was measured by BCA assay (Thermo Fisher, Waltham, MA, USA). 20 µg of protein lysate was run on an SDS-PAGE gel (Mini-PROTEAN TGX Precast Protein Gels, cat# 4561094, Bio-Rad), followed by protein transfer on a PVDF membrane. The antibodies used are β-Actin (cat# 4967 S), p-Chk2 (Thr68) (cat# 2197), p-ATM (Ser1981) (cat# 5883), p-Histone H2A.X (Ser139) (cat# 9718), c-Myc (cat# 13987 S) (CST), p53 (cat# sc-126) and p21 (cat# sc-53870) (Santa Cruz, Dallas, Texas US).

MYC T58A and MYC overexpression

PIG-MycT58A (cat# 177648) and pCW57.1 CMYC (Plasmid #164145) were purchased from Addgene to amplify and clone oncogenic and WT MYC into pLenti CMV Blast empty (w263-1) (cat# 17486) to generate pLenti CMV Blast MYC T58A. Lentivirus was produced from pLenti CMV Blast empty (control) and pLenti CMV Blast MYC T58A following the same protocol for CAR19 virus production. MYC T58A-expressing CART cells were selected with blasticidin (cat# A1113903, Thermo Fisher) at 10 µg/ml concentration between days 3–8 of CART manufacturing.

Telomere length measurements

DNA was isolated from T cells D0 and CART cells at D8 and D15 with the DNeasy Blood & Tissue Kit (QIAGEN) according to the manufacturer's protocol. Telomere length was measured by qPCR with the Absolute Human Telomere Length Quantification qPCR Assay Kit (cat#

8918, ScienCell Research Laboratories, Carlsbad, CA, USA) following the manufacturer's protocol.

Software

All statistics were performed using GraphPad Prism version 10.2.0 for Windows (GraphPad Software, La Jolla, CA, USA). Statistical tests are described in detail in the respective figure legends. Flow cytometry data were analyzed by FlowJo (Ashland, Oregon, US). Illustrations were generated by Biorender (Toronto, Ontario, Canada).

Results

A model to study irreversible CART cell dysfunction using recurrent activation followed by rest

We utilized an in vitro model that incorporates serial CART cell activation followed by resting periods between stimulations. Serial CART cell activation/resting cycles are intended to mimic multiple rounds of CART cell activation by recurrent interactions with cancer cells, while resting periods are implemented to enrich irreversible senescent CART cell populations [15–18]. We generated untransduced (UTD), BBζ, and 28ζ cells from healthy donor T cells from Day 0 (D0) to Day 8 (D8) (Supp. Fig. S1A). D8 CART cells served as a baseline timepoint for manufactured CART cell function and phenotype, as they are equivalent to freshly manufactured CART cells used in preclinical experiments and in clinical settings [9]. We activated both BBζ and 28ζ, which expressed similar levels of CAR (Supp. Fig. S1B), through repeated cocultures with lethally irradiated $CD19^+$ mantle cell lymphoma cell line JeKo-1, followed by a period of rest (Supp. Fig. S1A, D8 to D15). During rest, CART cells were cultured in T cell medium without additional target cells for four days prior to analysis. CART cells after one activation/rest cycle in this report are referred to as activated/rested or Day 15 (D15) CART cells.

In this model, we found that the expression of inhibitory receptors — lymphocyte activation gene 3 (LAG-3), cytotoxic T lymphocyte-associated protein 4 (CTLA-4), programmed cell death 1 (PD-1) and, T cell immunoglobulin and mucin domain 3 (TIM-3)—increased significantly three days after activation with anti-CD3/CD28 Dynabeads (used during CART cell production, Supp. Fig. S1A). LAG-3, CTLA-4, and PD-1 returned to baseline levels on D8, after two days of rest. TIM-3, however, remained elevated following activation and rest (Supp. Fig. S1C). Similarly, LAG-3, CTLA-4, and PD-1 all returned to basal levels at the end of each activation/rest cycle (Supp. Fig. S1D-F), but TIM-3 remained persistently elevated even after resting periods (Supp. Fig. S1G). Persistent TIM-3 expression is reported to be associated with senescent T cells [37].

Recurrent activation impairs CART cell activity and cytokine profile in vitro and in vivo

We next tested the effect of recurrent CART cell activation on CART cell efficacy in vitro and in vivo. We cocultured BBζ and 28ζ cells at baseline D8 and activated/rested D15 with JeKo-1 in vitro to measure CART cell activation. Both BBζ and 28ζ cells demonstrated decreased killing (Fig. 1A), number of cells entering cell cycle (Fig. 1B), and antigen-specific proliferation (Fig. 1C) after coculture. These findings were consistent when CART19 cells were cocultured with the acute lymphoblastic leukemia cell line, NALM6, as well (Supp. Fig. S2A, B). Collectively, our data indicate that recurrently activated/rested CART19 cells are associated with impaired effector functions without overt upregulation of exhaustion markers but with persistent TIM3 expression, suggestive of a senescent phenotype. 28ζ efficacy was impaired more by recurrent activation/resting compared to BBζ. This is consistent with other studies demonstrating that 28ζ exhibit stronger initial activation which lasts for shorter periods of time [19, 38, 39].

To further investigate these findings, recurrently activated CART19 cells were tested in a xenograft lymphoma mouse model. We intravenously engrafted 1×10^6 $luciferase^+$ JeKo-1 cells to NOD-SCID-IL2rγ$^{-/-}$ (NSG) mice. When bioluminescence intensity of the tumor cells reached ~ 10^8 photons/second, mice were randomized by tumor burden and treated intravenously with 1×10^6 UTD control or with BBζ or 28ζ cells that were previously cryopreserved at baseline or after activation/rest (Fig. 1D). Mice treated with baseline BBζ D8 or 28ζ D8 had significantly lower tumor burden compared to UTD-treated mice. However, in both recurrently activated/rested BBζ D15- and 28ζ D15-treated mice, tumor burdens were not significantly different from UTD-treated mice (Fig. 1E, F), and survival decreased in both BBζ D15- and 28ζ D15-treated mice (Supp. Fig. S2C), indicating pronounced CART dysfunction in recurrently activated/rested CART cells.

Secretion of tumor necrosis factor (TNF)-α has been reported to be elevated in senescent T cells [40]. Therefore, we measured TNF-α levels from the serum of mice from our in vivo model. Serum levels of TNF-α were significantly elevated in activated/rested BBζ-treated mice compared to baseline BBζ-treated mice, but this trend was not observed in 28ζ-treated mice (Fig. 1G).

Senescence-like immunophenotype in CART cells differs based on costimulatory domain

To further characterize the development of a senescence-like phenotype in CART19 cells, we next assessed levels of senescence markers in our recurrently activated/rested CART cells by flow cytometry, qPCR, telomere length, and DNA damage markers. p21 expression is an early

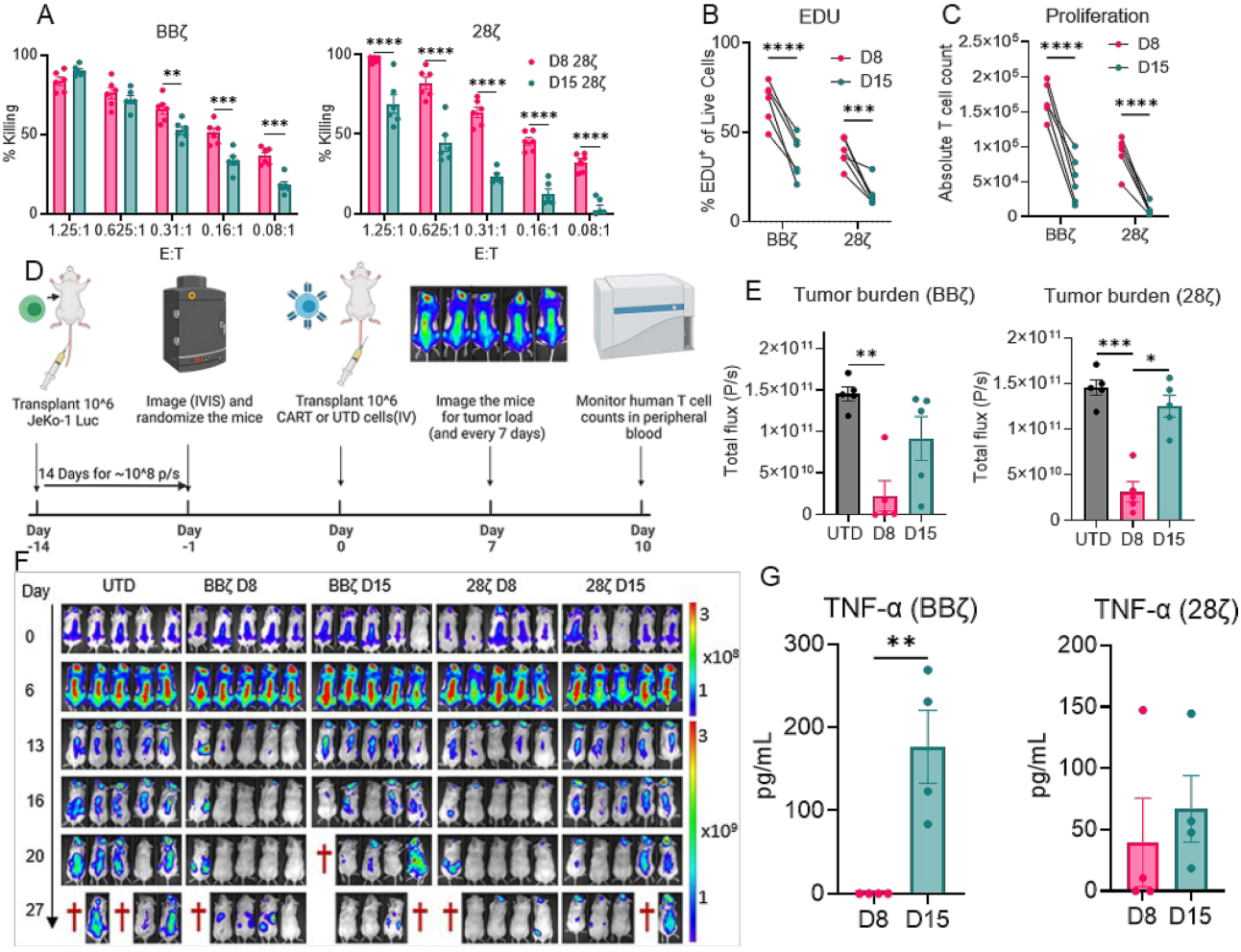

Fig. 1 Recurrent activation/resting impairs CART cell activity. **A-C.** D8 CART cells are generated and serially activated/rested to produce D15 CART cells as indicated in Supp. Fig. S1A. CART cells at each time point are cocultured with JeKo-1 to measure (**A.**) antigen-specific killing two days after coculture, (**B.**) cells entering cell cycle after 24 h of activation and (**C.**) CART cell proliferation three days after coculture. **D.** Summary of the in vivo experiments. Mice were intravenously engrafted with 1×10^6 luciferase + JeKo-1 cells. After JeKo-1 tumor burden reached ~ 10^8 photons/second, mice received 1×10^6-1.5×10^6 UTD or CART cells intravenously as indicated in each group. Tumor burden was serially assessed via bioluminescence ($n = 5$ mice/group). **E-F.** Tumor burden, measured by bioluminescence imaging, 16 days post-CART cell injection is shown (one-way ANOVA). **G.** Peripheral blood samples from mice were collected 21 days after CART cell infusion. Serum levels of TNF-α (one-way ANOVA) are plotted. Error bars, SEM. ns $p > 0.05$, *$p < 0.05$, **$p < 0.01$, ***$p < 0.001$, ****$p < 0.0001$

senescence event [31]. The amount of p21$^+$ CART cells increased significantly in repeatedly activated/rested BBζ compared to 28ζ at both baseline D8 and activated/rested D15 (Fig. 2A). T cell senescence marker KLRG1 expression was higher in BBζ compared to 28ζ at D15. While KLRG1 levels remained similar in BBζ at D8 and D15, the amount of KLRG1-expressing 28ζ cells decreased at D15 compared to D8 (Fig. 2B). uPAR has recently been identified as a surface marker for senescent cells [41, 42]. uPAR levels were higher in both baseline and activated/rested BBζ cells compared to 28ζ (Fig. 2C). CD27 expression decreased in both BBζ and 28ζ upon recurrent activation (Fig. 2D). TIM-3 levels (Fig. 2E) were higher in baseline BBζ compared to 28ζ. Since CD4:CD8 ratio is variable from one donor to the other, we measured the expression of senescence markers in CD4$^+$ and CD8$^+$ CART cells for both BBζ and 28ζ (Supp. Fig. S3A, B). uPAR and KLRG1 were similarly upregulated in BBζ compared to 28ζ in both CD4$^+$ and CD8$^+$ CART cells. To further evaluate the potential impact of CD4:CD8 ratio on the development of senescence phenotype, we sorted CD8$^+$ and CD4$^+$ CART cells with microbeads and mixed them at 1:1 ratio (referred to as BBζ 1:1 and 28ζ 1:1) in an independent cohort ($n = 4$). CART cells are stained for CD4 and CD8 after 1:1 mixing, (Supp. Fig. S3C). Expression of uPAR and KLRG1 was higher in BBζ compared to 28ζ in the CART cells with fixed 1:1 CD4:CD8 ratio, as well as in the CD4$^+$ and CD8$^+$ CART cell fractions (Supp. Fig S3D-E), similar to the phenotype of CART cells generated from variable CD4:CD8 ratios. Finally, we

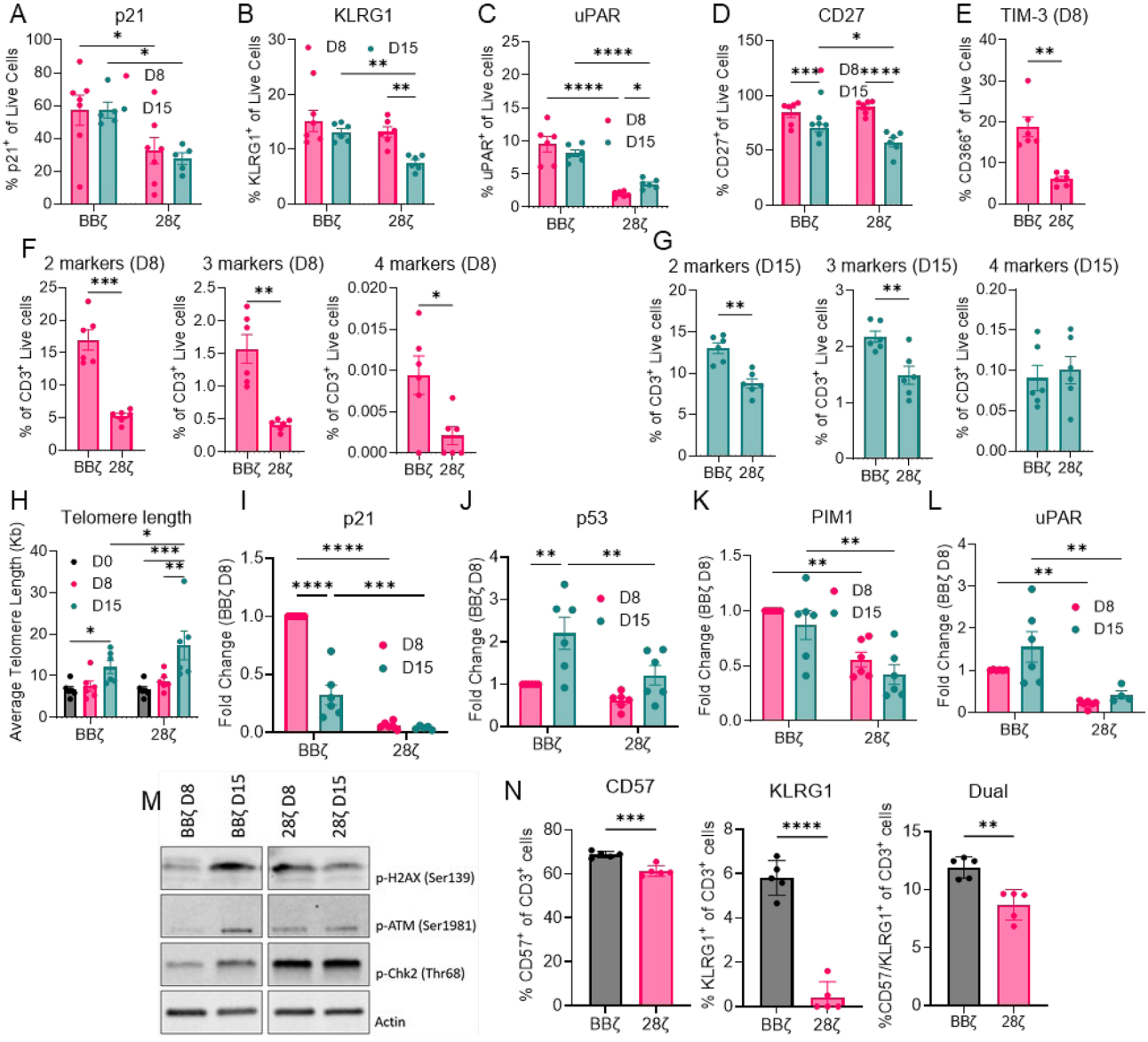

Fig. 2 Recurrent activation/rest differentially induced senescence in CART cells with alternative costimulatory domains. **A-E.** The percentage of $CD3^+$ T cells that are positive for (**A.**) p21, (**B.**) KLRG1, (**C.**) uPAR, (**D.**) CD27 and (**E.**) TIM-3 as measured by flow cytometry are plotted ($n = 6$ donors) (A-D., two-way ANOVA, E., t-test). **F-G.** Expression of uPAR, TIM-3, and KLRG1 and loss of CD27 expression are considered senescence events. Simultaneous occurrence of two, three, and four of these events in (**F.**) D8 and (**G.**) D15 CART cells are plotted as percent of $CD3^+$ cells (t-test). **H.** DNA is isolated from D0, D8 and D15 CART cells. The telomere lengths are measured by qPCR and plotted for each time point (two-way ANOVA). **I-L.** mRNA expression of (**I.**) p21, (**J.**) p53, (**K.**) PIM-1, and (**L.**) uPAR are measured by qPCR. Fold change is calculated by 2^{-} (–delta delta CT). The expression levels are normalized to BBζ D8 (two-way ANOVA). **M.** Recurrently activated CART cells were immunoblotted for DNA damage markers p-H2AX (Ser139), p-ATM (Ser1981), and p-Chk2 (Thr68). **N.** NSG mice received JeKo-1, were randomized, and received BBζ and 28ζ. The spleens from mice were collected and flowed for the indicated markers 21 days after CART injection ($n = 3$, t-test). Error bars, SEM. $^*p < 0.05$, $^{**}p < 0.01$, $^{***}p < 0.001$

assessed the antitumor killing of BBζ and 28ζ CART with 1:1 CD4:CD8 ratio following repeated cycles of activation/rest, to determine if CD4:CD8 ratio contributes to senescence induced CART cell failure. Baseline CART cells on D8 or activated/rested CART cells on D15 were cocultured with luciferase positive JeKo-1 cells for 24 h at the indicated E: T ratios. The antigen-specific killing of both BBζ 1:1 and 28ζ 1:1 was negatively impacted following recurrent activation (Fig S3F-G). The killing of recurrently activated/rested CART cells with variable CD4:CD8 ratios was similar to the killing of recurrently activated/rested CART cells with 1:1 CD4:CD8 ratio (Fig. S3H-I).

T cell activation, senescence and exhaustion are closely related but distinct T cell phenotypes. Several proteins are identified to be expressed in both senescence

and exhaustion in different studies [21, 37, 43–46]. We therefore analyzed the simultaneous co-expression of two or more senescence-associated receptors on CART cells, including the overexpression of uPAR, TIM-3, and KLRG1, or the loss of CD27 expression to more stringently define CART senescence [18, 41]. Percentages of cells which displayed multiple senescence-related protein expression were significantly higher in BBζ compared to 28ζ as early as D8 (Fig. 2F) as well as on D15 (Fig. 2G). Interestingly, when co-expression of the 4 markers was examined, both D15 BBζ and 28ζ exhibited similar levels of expression. This is possibly because 28ζ also develop some degree of senescence by D15 of repeated stimulation/rest cycles (Fig. 2G).

As shorter telomere length is a hallmark of cell senescence, we next measured telomere length of T cells at D0 and CART cells at D8 and D15 by qPCR. Interestingly, telomere lengths were increased in both BBζ and 28ζ upon activation (Fig. 2H). T cell activation is known to induce human telomerase reverse transcriptase (hTERT) activity and telomere elongation upon activation [47]. However, telomere length of BBζ was significantly shorter than 28ζ at D15, further supporting a more prominent senescent phenotype in BBζ (Fig. 2H).

We then analyzed the expression of cell cycle regulators and senescence markers as additional measures of senescence by qPCR. In accordance with our flow cytometry analysis, we found increased p21 expression in BBζ compared to 28ζ at both D8 and D15 (Fig. 2I). Likewise, p53 expression increased in recurrently activated BBζ and in BBζ D15 compared to 28ζ D15 (Fig. 2J). Expression of both PIM1 (Fig. 2K) and uPAR (Fig. 2L) was higher in BBζ compared to 28ζ at both D8 and D15.

Next, we evaluated recurrently activated/rested CART cells for upregulation of well-established DNA damage markers by immunoblotting, since DNA damage is a major inducer and marker of senescence [48]. Our results indicated that levels of DNA damage markers p-H2AX (Ser139), p-ATM (Ser1981), and p-Chk2 (Thr68) are upregulated upon repeated activation in BBζ but not in 28ζ (Fig. 2M). CART cells isolated from the spleens of mice 21 days following CART injection (Fig. 1D) demonstrated higher expression of KLRG1 and/or CD57 in BBζ compared to 28ζ, again indicating a more prominent senescent phenotype in BBζ in vivo (Fig. 2N).

A senescent transcriptional signature is differentially enriched upon recurrent activation/rest cycles in BBζ vs. 28ζ

Next, we assessed the transcriptome of recurrently activated/rested CART cells from three healthy donors by performing RNA sequencing as illustrated in Supp. Fig. S1A. CART cells from different donors clustered based on the costimulatory domain rather than clustering by donor or D0, D8, and D15 in principal component analysis (PCA) (Supp. Fig. S4A). D15 CART cells were clustered based on costimulatory domain in unsupervised hierarchical clustering analysis based on the expression of the genes listed in senMayo gene set (Supp. Fig. S4B). Gene set enrichment analysis (GSEA) with a focus on senMayo, a novel gene set specific for senescent cells [49] was significantly enriched activated/rested BBζ but not 28ζ (Fig. 3A). Normalized gene counts in hallmark gene sets revealed enriched gene sets in activated/rested BBζ related to senescent T cell phenotypes, including DNA damage, oxidative stress, and glycolysis (Supp. Fig. S4C, Supp. Table S1). Next, we compared basal or repeatedly activated/rested BBζ and 28ζ to determine differentially expressed genes and compare them with senescence-associated genes listed in CellAge (https://genomics.senescence.info/cells/) [50]. We found an upregulation in genes that are reported to induce senescence and a downregulation of genes that are reported to inhibit senescence, particularly in BBζ (Fig. 3B). Collectively, our data suggest that both BBζ and 28ζ exhibit signs of senescence as evident by impaired effector functions, persistent elevation of TIM-3, increased secretion of inflammatory cytokines, and increased cell cycle regulator expression upon repeated stimulation followed by rest. However, our experiments strongly indicate that BBζ are more susceptible to senescence as indicated by their significant senescence-associated markers, accumulated DNA damage markers, telomere length, and enrichment of senescence gene signature.

MYC activation due to recurrent activation/resting cycles has differential impacts on BBζ and 28ζ

GSEA revealed that numerous MYC-related gene sets were enriched in BBζ but depleted in 28ζ following repeated activation/rest cycles (Fig. 3C, Supp. Tables S1–S2). We therefore measured MYC expression in recurrently activated/rested CART cells and found that MYC was significantly upregulated in BBζ but decreased in 28ζ upon recurrent activation/resting (Fig. 3D).

To test whether MYC activation differentially impacts BBζ and 28ζ, we transduced CART cells to overexpress oncogenic MYC T58A (MYC OE) and confirmed MYC overexpression compared to controls by qPCR (Fig. 4A). MYC and MYC T58A are known oncogenes, and acute oncogene activation in primary cells is a well-known inducer of senescence defined as oncogene-induced senescence [51]. Indeed, MYC activation upregulated known T cell senescence markers, such as p21, p53, and p-H2AX, in both BBζ and 28ζ as determined by immunoblotting or flow cytometric analysis (Fig. 4B, C). It should be noted that MYC overexpression in both BBζ and 28ζ induced a senescence phenotype (Fig. 4A-C). Notably, MYC activation did

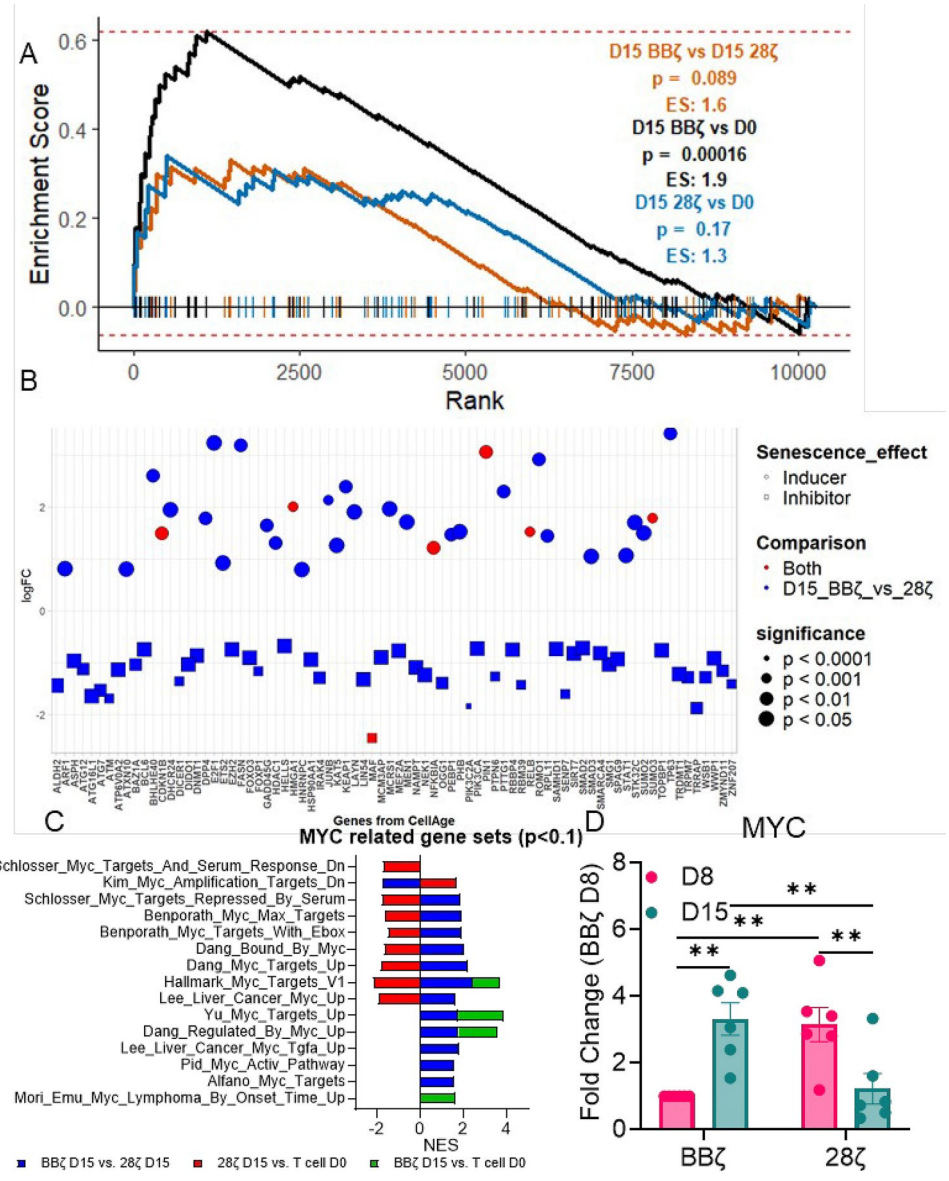

Fig. 3 Transcriptome analysis with recurrently activated/rested CART cells indicates a more prominent senescence-like phenotype in BBζ. **(A)** senMayo gene set enrichment is shown for the indicated CART groups. **(B)** Genes whose expression is significantly increased or decreased in BBζ compared to 28ζ at D8 and D15 are determined by differential gene expression (DGE) analysis. CellAge database lists genes that induce or inhibit senescence. The genes that induce senescence that are also overexpressed in BBζ, and genes that inhibit senescence that are also downregulated in BBζ are indicated. **(C)** Significantly enriched or depleted MYC-associated gene sets in recurrently activated/rested CART cells ($p < 0.1$) from GO and curated databases are shown. **(D)** MYC expression in recurrently activated CART cells are measured by qPCR. Fold change is calculated by 2^ (–delta delta CT). The expression levels are normalized to BBζ D8 (two-way ANOVA). $^{**}p < 0.01$

not induce exhaustion marker expression (Supp. Fig. S4D-F). Antigen-specific stimulation of BBζ MYC OE, but not 28ζ MYC OE, resulted in decreased cell cycle, measured with EDU, compared to control BBζ and 28ζ (Fig. 4D). BBζ MYC OE, but not 28ζ MYC OE, displayed decreased antigen-specific killing and proliferation compared to controls (Fig. 4E, F). These data suggest that MYC is activated in recurrently activated/rested BBζ, and MYC-induced senescence may have a detrimental impact on BBζ functions. To test the efficacy of wild type MYC-overexpressing CART cells in an in vivo setting, we performed a xenograft mice experiment similar to Fig. 1D. Here, JeKo-1-engrafted mice received 1.5×10^6 control or MYC overexpressing BBζ or 28ζ. Interestingly, the number of circulating CART cells in peripheral blood of both BBζ and 28ζ decreased upon MYC overexpression (Fig. 4G). This suggests that both 28ζ and BBζ might be negatively impacted by MYC overexpression (Fig. 4D-G). However, BBζ MYC OE was more profoundly impacted than MYC OE 28ζ (Fig. 4G), suggesting

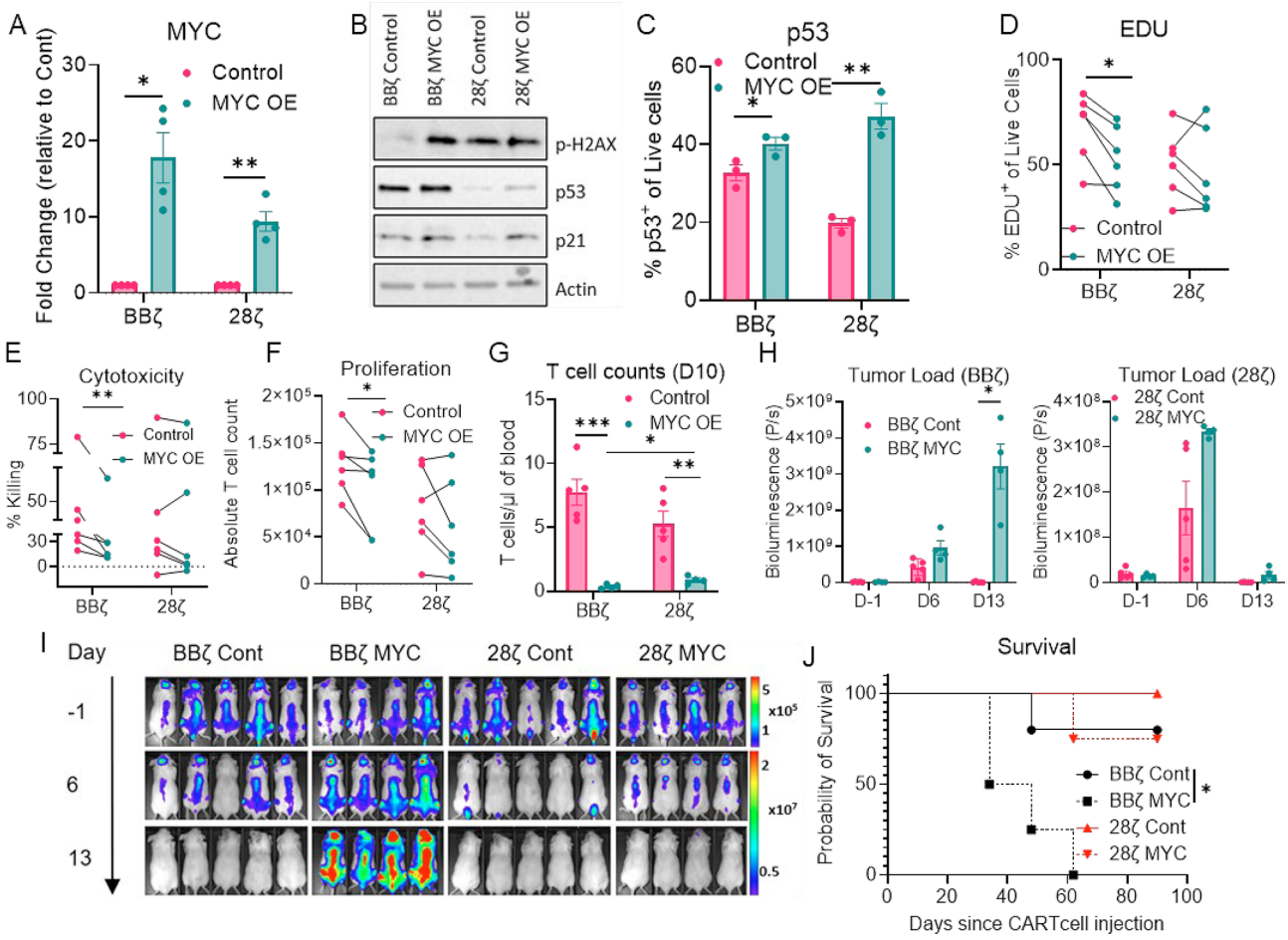

Fig. 4 Recurrent activation/rest induces senescence through MYC activation in BBζ. **A.** MYC is overexpressed in CART cells through lentiviral transduction. MYC expression is measured by qPCR. Fold change is calculated by 2^ (–delta delta CT). The expression levels are normalized to control (Cont) for each CART cell type. **B**. DNA damage and senescence makers are measured by immunoblotting of the indicated CART groups (representative of two donors). **C.** p53 levels of indicated CART groups as measured by flow cytometry are shown. (t-test, error bars, SEM, three technical replicates). **D-F.** MYC OE CART cells were cocultured with JeKo-1 cells. Cycling cells were measured by (**D.**) EDU, (**E.**) cytotoxicity, and (**F.**) proliferation (t-test, each point represents the average of three technical replicates from individual biological donors). **G.** JeKo-1-bearing mice received control or wildtype MYC-overexpressing CART cells. Peripheral blood samples are collected from mice to measure the number of circulating CART cells (t-test). **H-I.** The tumor burdens measured by bioluminescence were assessed weekly (two-way ANOVA). *$p < 0.05$, **$p < 0.01$, ***$p < 0.001$. **J.** Kaplan-Meier survival curve with MYC OE vs. Cont CART cells are shown (Log-rank test). Error bars, SEM. *$p < 0.05$, **$p < 0.01$

that BBζ is more sensitive to MYC activation. BBζ MYC OE-treated mice had significantly higher tumor burden compared to control BBζ mice as early as 13 days after CART cell injection, while this trend was not observed in 28ζ groups (Fig. 4H, I). BBζ MYC OE treated mice had a significantly worse overall survival compared to control mice (Fig. 4J).

Induction of senescence through irradiation enhances 28ζ

To further validate the effect of senescence on CART efficacy in BBζ and 28ζ, we next induced senescence in CART cells through sublethal irradiation on Day 2 of CART manufacturing (Supp. Fig. S5A). Irradiated CART cells showed increased senescence marker expression by qPCR (Fig. 5A-D) and flow cytometry (Supp. Fig. S5B-E). It should be noted that the yield of irradiated CART cells was ~10 times lower than non-irradiated CART cells (data not shown). Interestingly, upon co-culture with target cells, irradiated 28ζ, but not irradiated BBζ, killed target cells and entered the cell cycle more efficiently as measured by EDU assay (Fig. 5E-F). These phenomena, notably, occurred in irradiated 28ζ without a corresponding increase in proliferation (Fig. 5G). Since our experiments demonstrate that induction of a senescence-like state in CART cells impaired BBζ activity, but not 28ζ activity, we next assessed the potential impact of senescence on CART activity in the clinic. Analysis of publicly available single cell RNA sequencing datasets from patients treated with CART cells indicated that the senMayo gene set was enriched in non-responders vs. responders to tisagenlecleucel (tisa-cel, equivalent to BBζ), but not in non-responders vs. responders to

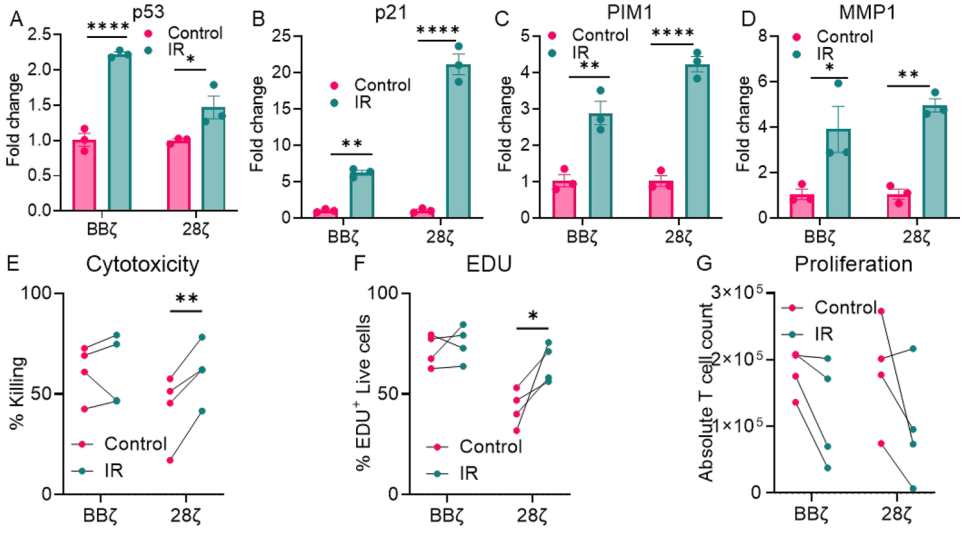

Fig. 5 Irradiation (IR)-induced senescence has opposing impact on CART cells with differing costimulatory domains in vitro and in vivo. **A-D.** Senescent CART cells were produced from irradiated T cells (3 Gy). RNA is isolated from D8 CART cells which was used in qPCR for indicated senescence markers. (One-way ANOVA; error bars, SEM, three technical replicates. Fold change is calculated by 2^ (–delta delta CT) method and irradiated BBζ and 28ζ are normalized to their respective control groups). **E-G.** Irradiated CART cells were cocultured with JeKo-1 cells and assessed for (**E.**) target cell killing, (**F.**) cell entering cell cycle, and (**G.**) proliferation. $n = 4$ donors, t-test, each point represents the average of three technical replicates from an individual biological donor. *$p < 0.05$, **$p < 0.01$, ****$p < 0.0001$

axicabtagene ciloleucel (axi-cel, equivalent to 28ζ), providing additional support for the role of senescence in the failure of 4-1BB- but not CD28-costimulated CART cells in the clinic (Fig. 6A). We generated a scoring system based on each patient's senMayo gene expression signature. Interestingly, axi-cel-treated but not tisa-cel-treated patients with high senMayo scores had longer progression-free survival (Fig. 6B) [25]. Similar to recurrently activated/rested BBζ (Fig. 3C), numerous MYC-related pathways were enriched in non-responders vs. responders to tisa-cel but not in non-responders vs. responders to axi-cel (Fig. 6C, Supp. Table S3) [25]. While these results were surprising, another recent study also found a positive correlation between presence of senescent-like axi-cel CART cells in patient peripheral blood and complete response, providing additional support for our findings [26]. Altogether, these data support the role of MYC-induced senescence in the failure of 41BB- but not CD28-costimulated CART cells.

Discussion

The goal of this study is to assess the role of senescence in CART cell dysfunction and its implications in the clinic. CART cells that were subjected to repeated cycles of activation/rest developed a state of senescence, which was more prominent in 41BB-costimulated CART cells. Transcriptomic analyses highlighted enrichment of MYC targets in recurrently activated/rested BBζ but not in 28ζ. As such, we induced senescence by overexpressing oncogenic MYC T58A or wild type MYC or by irradiation of CART cells and found that induction of senescence impacted BBζ and 28ζ efficacy differently in these models as well. Finally, our analysis indicated that senescence was associated with poor response with BBζ but not 28ζ in the clinic.

The development of senescence is characterized by upregulation of genes and markers that are also associated with T cell activation, exhaustion, or differentiation. To clearly differentiate senescence from other cellular fates, we utilized a multi-faceted approach which included cellular immunophenotype, functional profile, DNA damage assessment, telomere length, and transcriptomic profile after a resting period. We utilized a novel gene set for senescence that was recently reported, senMayo, which consists of 125 genes whose expression is consistently associated with senescence of multiple tissues induced through different methods [49]. senMayo gene set was notably enriched in recurrently activated/rested BBζ and in nonresponsive tisa-cel-treated patients but not in recurrently activated/rested 28ζ or nonresponsive axi-cel-treated patients.

T cell exhaustion has been demonstrated as a mechanism for CART cell failure in the clinic by several independent studies [12, 52–54]. T cell exhaustion is a reversible fate, and multiple genes have been shown to be involved in CART cell exhaustion [15, 18, 19]. Attempts to modulate CART cell exhaustion are in early-stage clinical testing. However, targeting exhaustion does not seem to be sufficient to fully reverse CART cell dysfunction or induce durable responses [55]. T cell senescence, on the other hand, is a permanent fate. CART cells have been shown to differentiate into different cellular fates based

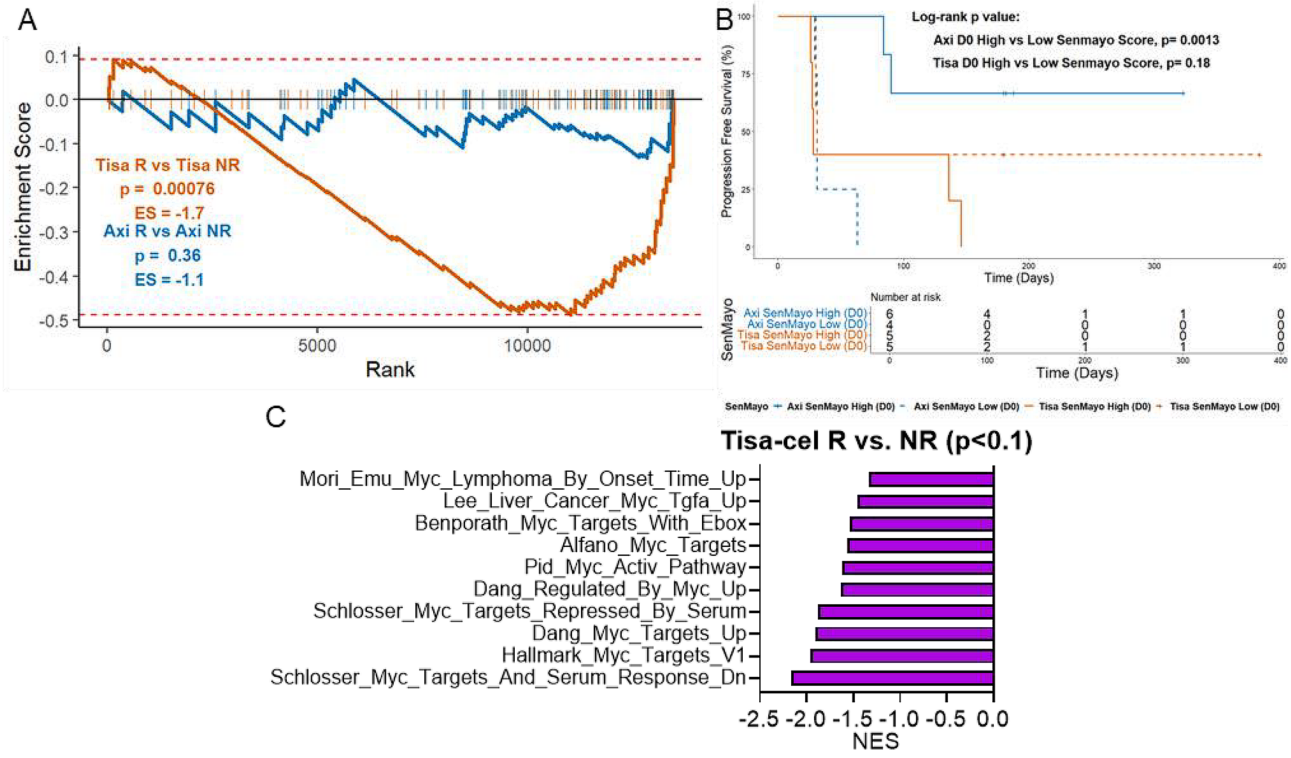

Fig. 6 Senescence has disparate impacts on CART cells with differing costimulatory domains in the clinic. **(A)** Axi-cel- and tisa-cel-treated patients are clustered as responsive and nonresponsive in a recently published patient dataset. senMayo gene set enrichment in nonresponsive tisa-cel is shown. **(B)** Genes belonging to senMayo gene sets are converted to gene score based on the expression of genes in senMayo, and then the patients are divided into senMayo high and low groups. Kaplan-Meier progression-free survival curve is shown (Log-rank test). **(C)** MYC-related gene set enrichment is shown in non-responsive tisa-cel-treated patients. (R: responsive, NR: nonresponsive)

on stimulatory signals. Based on these observations, we hypothesized that CART cells may be susceptible to a senescent-like phenotype following repeated interactions with cancer cells which cause CART cell therapy failure. Therefore, modulating CART cell senescence as well as exhaustion should both be considered to promote durable CART cell response.

To test our hypothesis, we utilized three independent strategies to mimic the induction of senescence in CART cells: repeated cycles of activation followed by rest, MYC overexpression, and irradiation. Our data strongly indicate the development of a state of senescence that is more profound and associated with impaired functions in 41BB-costimulated CART cells than CD28-costimulated CART cells in vitro, in vivo, and in the clinic. The development of senescence is independent of $CD4^+$ and $CD8^+$ composition of the CART cells. Early signs of senescence in BBζ were evident starting in D8 CART cells by elevated p21 (an early event in senescence [31]), and CD366 expressions. Extended activation/rest cycles have been shown to induce severe T cell dysfunction, which may result in more global T cell changes, masking the genes associated with senescence [12]. None of the strategies employed to induce senescence instigated an overt development of an exhaustion phenotype.

Our transcriptomic analysis highlighted significantly altered senescence-related genes in BBζ compared to 28ζ. *ABCB1* [57], *TRAF5* [58], and *ITGA1* [59], the absence of which are linked to T cell senescence and dysfunction, were downregulated in BBζ D15 compared to 28ζ D15. On the other hand, expression of senescence-associated genes, including *HMGB1*[60–63], *RELB* [63], *E2F1* [65], *TIGIT* [65, 66] and *CDH1* [68], were increased in BBζ D15 compared to 28ζ D15 (Supp. Tab. 4). Moreover, our transcriptomics analysis highlighted numerous senescence-inducing genes overexpressed and senescence-inhibiting genes downregulated in recurrently activated/rested BBζ according to the CellAge database, which highlights genes that are associated with senescence (Supp. Tab. 5).

Our analysis of published patient datasets [25] also supported enrichment of a senescence signature in non-responders to tisa-cel only. Surprisingly, our analyses showed that axi-cel-treated patients who had higher senescence scores had longer progression-free survival [26]. While these results were unexpected, these data are in alignment with previously published data; in an independent axi-cel-treated patient cohort, another group positively correlated the presence of senescent-like 28ζ cells in the peripheral blood one week after CART-cell

infusion with long term complete response. Additionally, the patient cohort published by Haradhvala et al. [25]. represented an ideal cohort for us to validate our findings, as they compared responders and nonresponders from both tisa-cel and axi-cel within the same study, albeit with relatively low patient numbers in each cohort. Follow up studies to validate our findings with larger groups of patients are planned in the future.

Our results support the possibility of novel strategies to ensure durable CART cell efficacy. Senolytics are a group of drugs which can selectively eliminate senesced cells. Our data provide rationale to include senolytic treatment during BBζ ex vivo production and/or to supplement BBζ with senolytics during treatment in vivo. Conversely, our results and findings from publicly available patient data sets suggest that 28ζ would not benefit from eliminating senesced CART cells as notably as BBζ. In addition to combination therapy with senolytics, modulating uPAR offers another strategy to improve CART cell efficacy through reducing senescence. uPAR is defined as a surface marker for senescent cells. Recently, $uPAR^+$ cells were eliminated through uPAR-specific CART cells in mice, resulting in less pronounced aging phenotypes [41, 42]. Aligned with these findings, we showed that BBζ expresses uPAR and PLAUR (the gene encoding uPAR) higher than 28ζ, providing an alternative strategy to selectively remove senescent CART cells. Additionally, identifying specific MYC targets which contribute to BBζ failure could lead to the development of a more durable CART cell therapy. For example, in a recent report, CART fitness was improved by treating pre- and post-infusion BBζ from chronic lymphocytic leukemia non-responders as well as lymphocytes during CART production with JQ-1, which downregulates MYC expression through BET inhibition [68]. Our data corroborate these findings and indicate the development of a senescent phenotype following MYC overexpression in both 28ζ and BBζ.

Given the complexity of senescence development, each of the three senescence models we tested highlighted different phenotypical, functional, and transcriptomic changes associated with senescence [31, 41]. We observed similar and specific senescence-associated changes BBζ and 28ζ when senescence was induced with irradiation, MYC overexpression, and repeated activation/rest cycles. Here, functional outcomes of senescence induction were similar across multiple independent methods. Recurrent activation induced impaired activity in both BBζ and 28ζ but induced senescence in BBζ more prominently. MYC oncogene-induced senescence resulted in BBζ dysfunction while irradiation-induced senescence improved 28ζ activity, supporting clinical correlative data here and published elsewhere [25]. The finding that MYC overexpression impacts CART cell differently based on their costimulatory domain is intriguing. It has become recently evident that mechanisms of failure in BBζ and 28ζ are different. A recent study suggests that BBζ failure is at least partly mediated by FOXO3 [70]. It is possible that MYC interacts directly with the FOXO3 pathway and that cross talks between MYC and FOXO3 [71] mediate senescence in BBζ. Finally, there is increasing evidence about the role of mitochondria in T cell aging and function. Resting BBζ have been shown to have higher mitochondrial content compared to 28ζ [72], but the impact of mitochondria on CART cell senescence is unknown. Considering the role of MYC in mitochondrial biogenesis [72] it is possible that mitochondria plays a role in differing senescence responses in BBζ and 28ζ. Work to further understand the interactions between mitochondria, MYC, and CART cell senescence is ongoing in the laboratory and will be reported in a subsequent manuscript.

Our findings demonstrate that repeated activation/resting cycles can serve as a relevant model to study senescent-like phenotypes and CART cell failure in an in vitro setting. Our activation/rest model has the potential to identify additional genes that are associated with senescence and therapeutic targets to ameliorate CART cell failure as a fast, reliable, and low-cost in vitro testing platform. We chose CART19 as a model to study senescence due to its clinical relevance. Further experiments are needed to determine whether these differences are applicable to other CAR constructs and tumor models.

In summary, our study demonstrates that CART cells are susceptible to senescence, which may be a predominant mechanism of failure in 41BB-costimulated but not CD28-costimulated CART cells. These findings shed light on important mechanisms underlying the emergence of senescence in CART cells across different costimulatory domains. They also highlight the potential of new therapeutic strategies to improve CART cell function through targeting senescent CART cells while considering differences based on CART costimulation.

Supplementary Information

The online version contains supplementary material available at https://doi.org/10.1186/s12943-025-02371-1.

Supplementary Material 1

Supplementary Material 2

Supplementary Material 3

Supplementary Material 4

Supplementary Material 5

Supplementary Material 6

Acknowledgements

This study was partly funded by Regenerative Medicine Minnesota RMM 072523 TR 004 (IC), Mayo Clinic Division of Hematology (IC), Eagles 5th District Cancer Telethon Funds for Cancer Research (IC), Mayo Clinic Center

for Individualized Medicine (SSK), Mayo Clinic Comprehensive Cancer Center (SKK), Mayo Clinic Center for Regenerative Biotherapeutics (SSK), National Institutes of Health R37CA266344 (SSK) and R01AI179974 (SSK), and Department of Defense grant CA201127 (SSK), Predolin Foundation (RLS and SSK). We would like to thank Michael W. and Georgia Taylor Michelson for their funding contribution that assisted in supporting this project.

Author contributions

Experimental design, Conceptualization: IC, SSK. Perform experiments: IC, BLK, LKM, RLS. Analyze data: IC, BA, FS, HAE, SSK. Contribute reagents: SSK, IC, RLS. Supervision: SSK. Writing - original draft: SSK, IC, ELS. Writing - review & editing: IC, ELS, OLS, CMR, KY, CMS, JMF, MLR, OLGR, JHG, EJO, TNH, BLK, LKM, MH, LKF, HX, IH, BA, FS, HAE, RLS, SSK.

Data availability

The raw and processed files from RNA sequencing of T cells (D0), baseline (D8) and recurrently activated rested BBζ and 28ζ (D15) are available in GEO under accession code GSE290151.

Declarations

Ethics approval and consent to participate

The use of recombinant DNA in the laboratory was approved by the Mayo Clinic Institutional Biosafety Committee (IBC), IBC number HIP00000252.43. Animal studies were performed according to the Institutional Animal Care and Use Committee (IACUC) at the Mayo Clinic animal facilities (IACUC # A00001767-16-R22).

Competing interests

SSK is an inventor on patents in the field of CAR immunotherapy that are licensed to Novartis (through an agreement between Mayo Clinic, University of Pennsylvania, and Novartis), and MustangBio (through Mayo Clinic). RLS, and SSK are inventors on patents in the field of CAR immunotherapy that are licensed to Humanigen/Taran (through Mayo Clinic). IC, ELS, OLS, CMR, KY, CMS, JMF, OGR, TNH, BLK, LKM, MH, HX, RLS and SSK are inventors on patents that are licensed to Immix Biopharma. SSK receives research funding from Kite, Gilead, Juno, BMS, Novartis, Humanigen, MorphoSys, Tolero, Sunesis/Viracta, LifEngine Animal Health Laboratories Inc, and Lentigen. SSK has participated in advisory meetings with Kite/Gilead, Humanigen, Juno/BMS, Capstan Bio, and Novartis. SSK has served on the data safety and monitoring board with Humanigen, and Carisma. SSK has severed a consultant for Torque, Calibr, Novartis, Kite, Capstan Bio, Luminary, Carisma, and Humanigen.

Received: 18 December 2024 / Accepted: 28 May 2025
Published online: 10 June 2025

References

1. Rodriguez-Cartagena LG, Bowles BS, Kurani SS, Windebank AJ, Kenderian SS, Greenberg-Worisek AJ. Chimeric antigen receptor T-Cells: successful translation of the first cell and gene therapy from bench to bedside. *Clinical and translational science*. Published Online September. 2018;22. https://doi.org/10.1111/cts.12586.
2. Brentjens RJ, Santos E, Nikhamin Y, et al. Genetically targeted T cells eradicate systemic acute lymphoblastic leukemia xenografts. Clin Cancer Res. 2007;13(18):5426–35. https://doi.org/10.1158/1078-0432.CCR-07-0674.
3. Maude SL, Laetsch TW, Buechner J, et al. Tisagenlecleucel in children and young adults with B-Cell lymphoblastic leukemia. N Engl J Med. 2018;378(5):439–48. https://doi.org/10.1056/NEJMoa1709866.
4. Fraietta JA, Lacey SF, Orlando EJ, et al. Determinants of response and resistance to CD19 chimeric antigen receptor (CAR) T cell therapy of chronic lymphocytic leukemia. Nat Med. 2018;24(5):563–71. https://doi.org/10.1038/s41591-018-0010-1.
5. Singh N, Lee YG, Shestova O, et al. Impaired death receptor signaling in leukemia causes antigen-independent resistance by inducing CAR T-cell dysfunction. Cancer Discov. 2020;10(4):552–67. https://doi.org/10.1158/2159-8290.CD-19-0813.
6. Can I, Cox MJ, Siegler EL, Sakemura R, Kenderian SS. Challenges of chimeric antigen receptor T-cell therapy in chronic lymphocytic leukemia: lessons learned. Exp Hematol. 2022;108:1–7. https://doi.org/10.1016/j.exphem.2022.02.001.
7. Cox MJ, Lucien-Matteoni F, Sakemura R, et al. Circulating extracellular vesicles induce chimeric antigen receptor T cell dysfunction in chronic lymphocytic leukemia (CLL). Biol Blood Marrow Transplant. 2020;26(3):S2–3. https://doi.org/10.1016/j.bbmt.2019.12.137.
8. Cox MJ, Manriquez Roman C, Tapper EE et al. GM-CSF disruption in CART cells modulates T cell activation and enhances CART cell anti-tumor activity. Leukemia 2022 36:6. 2022;36(6):1635–1645. https://doi.org/10.1038/s41375-022-01572-7
9. Sterner RM, Sakemura R, Cox MJ, et al. GM-CSF inhibition reduces cytokine release syndrome and neuroinflammation but enhances CAR-T cell function in xenografts. Blood. 2019;133(7):697–709. https://doi.org/10.1182/BLOOD-2018-10-881722.
10. Cox MJ, Lucien F, Sakemura R, et al. Leukemic extracellular vesicles induce chimeric antigen receptor T cell dysfunction in chronic lymphocytic leukemia. Mol Ther. 2021;29(4):1529–40. https://doi.org/10.1016/j.ymthe.2020.12.033.
11. Sakemura RL, Hefazi M, Cox MJ, et al. AXL inhibition improves the antitumor activity of chimeric antigen receptor T cells. Cancer Immunol Res. 2023;11(9):1222–36. https://doi.org/10.1158/2326-6066.CIR-22-0254.
12. Stewart CM, Siegler EL, Sakemura RL, et al. IL-4 drives exhaustion of CD8 + CART cells. Nat Commun. 2024;15(1):7921. https://doi.org/10.1038/s41467-024-51978-3.
13. Titov A, Kaminskiy Y, Ganeeva I, et al. Knowns and unknowns about CAR-T cell dysfunction. Cancers. 2022;14(4):1078. https://doi.org/10.3390/cancers14041078.
14. Wherry EJ, Ha SJ, Kaech SM, et al. Molecular signature of CD8 + T cell exhaustion during chronic viral infection. Immunity. 2007;27(4):670–84. https://doi.org/10.1016/J.IMMUNI.2007.09.006.
15. Blackburn SD, Shin H, Haining WN et al. Coregulation of CD8 + T cell exhaustion by multiple inhibitory receptors during chronic viral infection. Nature Immunology 2008;10(1):29–37. https://doi.org/10.1038/ni.1679
16. Tang L, Zhang Y, Hu Y, Mei H. T cell exhaustion and CAR-T immunotherapy in hematological malignancies. Biomed Res Int. 2021;2021. https://doi.org/10.1155/2021/6616391.
17. Lynn RC, Weber EW, Sotillo E, et al. c-Jun overexpression in CAR T cells induces exhaustion resistance. Nature. 2019;576(7786):293–300. https://doi.org/10.1038/s41586-019-1805-z.
18. Zhao Y, Shao Q, Peng G. Exhaustion and senescence: Two crucial dysfunctional states of T cells in the tumor microenvironment. Cell Mol Immunol. 2019; November. https://doi.org/10.1038/s41423-019-0344-8.
19. Long AH, Haso WM, Shern JF, et al. 4-1BB costimulation ameliorates T cell exhaustion induced by tonic signaling of chimeric antigen receptors. Nat Med. 2015;21(6):581–90. https://doi.org/10.1038/nm.3838.
20. Kasakovski D, Xu L, Li Y. T cell senescence and CAR-T cell exhaustion in hematological malignancies. J Hematol Oncol. 2018;11(1). https://doi.org/10.1186/s13045-018-0629-x.
21. Wherry EJ. T cell exhaustion. Nat Immunol. 2011;12(6):492–9. https://doi.org/10.1038/ni.2035.
22. Chou JP, Effros RB, T CELL REPLICATIVE, SENESCENCE IN HUMAN AGING. Curr Pharm Design. 2013;19(9):1680.
23. Baker DJ, Wijshake T, Tchkonia T, et al. Clearance of p16Ink4a-positive senescent cells delays ageing-associated disorders. Nature. 2011;479(7372):232–6. https://doi.org/10.1038/NATURE10600.
24. Naturally. occurring p16Ink4a-positive cells shorten healthy lifespan| Nature. Accessed August 27, 2024. https://www.nature.com/articles/nature16932
25. Haradhvala NJ, Leick MB, Maurer K et al. Distinct cellular dynamics associated with response to CAR-T therapy for refractory B cell lymphoma. Published online 1959. https://doi.org/10.1038/s41591-022-01959-0
26. Good Z, Spiegel JY, Sahaf B, et al. Post-infusion CAR treg cells identify patients resistant to CD19-CAR therapy. Nat Med. 2022;28(9):1860–71. https://doi.org/10.1038/s41591-022-01960-7.
27. Kowolik CM, Topp MS, Gonzalez S, et al. CD28 costimulation provided through a CD19-specific chimeric antigen receptor enhances in vivo persistence and antitumor efficacy of adoptively transferred T cells. Cancer Res. 2006;66(22):10995–1004. https://doi.org/10.1158/0008-5472.CAN-06-0160.
28. Cells CART, Connor RSO, Fraietta JA, et al. Distinct signaling of coreceptors regulates specific metabolism pathways and impacts memory article distinct signaling of coreceptors regulates specific metabolism pathways and impacts memory development in CAR T cells. Immunity. 2016;44(2):380–90. https://doi.org/10.1016/j.immuni.2016.01.021.

29. Gomes-Silva D, Mukherjee M, Srinivasan M, et al. Tonic 4-1BB costimulation in chimeric antigen receptors impedes T cell survival and is Vector-Dependent. Cell Rep. 2017;21(1):17–26. https://doi.org/10.1016/j.celrep.2017.09.015.
30. Sakemura R, Cox MJ, Hansen MJ, et al. Targeting Cancer associated fibroblasts in the bone marrow prevents resistance to chimeric antigen receptor T cell therapy in multiple myeloma. Blood. 2019;134(Supplement1):865–865. https://doi.org/10.1182/blood-2019-123277.
31. Sturmlechner I, Zhang C, Sine CC, et al. p21 produces a bioactive secretome that places stressed cells under immunosurveillance. Science. 2021;374(6567). https://doi.org/10.1126/science.abb3420.
32. Mollaoglu G, Guthrie MR, Böhm S, et al. MYC drives progression of small cell lung Cancer to a variant neuroendocrine subtype with vulnerability to Aurora kinase inhibition. Cancer Cell. 2017;31(2):270–85. https://doi.org/10.1016/j.ccell.2016.12.005.
33. Chen J, Zhang R, Xie M, Luan C, Li X. Transcriptome sequencing identifies PLAUR as an important player in patients with Dermatomyositis-Associated interstitial lung disease. Front Genet. 2021;12:784215. https://doi.org/10.3389/fgene.2021.784215.
34. Gao AY, Diaz Espinosa AM, Gianì F, et al. Pim-1 kinase is a positive feedback regulator of the senescent lung fibroblast inflammatory secretome. Am J Physiol Lung Cell Mol Physiol. 2022;323(6):L687–97. https://doi.org/10.1152/AJPLUNG.00023.2022.
35. Subramanian A, Tamayo P, Mootha VK et al. Gene set enrichment analysis: A knowledge-based approach for interpreting genome-wide expression profiles. Proceedings of the National Academy of Sciences. 2005;102(43):15545–15550. https://doi.org/10.1073/pnas.0506580102
36. Sakemura L, Clinic M, States U et al. CD19 occupancy with tafasitamab increases therapeutic index of CART19 cell therapy and diminishes severity of CRS. Published online 2022. https://doi.org/10.1182/blood.2022018905
37. Li H, Wu K, Tao K, et al. Tim-3/galectin-9 signaling pathway mediates T-cell dysfunction and predicts poor prognosis in patients with hepatitis B virus-associated hepatocellular carcinoma. Hepatology. 2012;56(4):1342–51. https://doi.org/10.1002/hep.25777.
38. Philipson BI, O'Connor RS, May MJ, June CH, Albelda SM, Milone MC. 4-1BB costimulation promotes CAR T cell survival through noncanonical NF-κB signaling. Sci Signal. 2020;13(625). https://doi.org/10.1126/scisignal.aay8248.
39. Jayaraman J, Mellody MP, Hou AJ, et al. CAR-T design: elements and their synergistic function. EBioMedicine. 2020;58:102931. https://doi.org/10.1016/j.ebiom.2020.102931.
40. Ye J, Huang X, Hsueh EC, et al. Human regulatory T cells induce T-lymphocyte senescence. Blood. 2012;120(10):2021–31. https://doi.org/10.1182/BLOOD-2012-03-416040.
41. Amor C, Feucht J, Leibold J et al. Senolytic CAR T cells reverse senescence-associated pathologies. Nature Published Online June 17, 2020:1–6. https://doi.org/10.1038/s41586-020-2403-9
42. Amor C, Fernández-Maestre I, Chowdhury S et al. Prophylactic and long-lasting efficacy of senolytic CAR T cells against age-related metabolic dysfunction. Nature Aging 2024. Published online January 24, 2024:1–14. https://doi.org/10.1038/s43587-023-00560-5
43. Wherry EJ, Kurachi M. Molecular and cellular insights into T cell exhaustion. Nat Rev Immunol. 2015;15(8):486–99. https://doi.org/10.1038/nri3862.
44. Janelle V, Neault M, Lebel MÈ, et al. p16INK4a regulates cellular senescence in PD-1-Expressing human T cells. Front Immunol. 2021;12. https://doi.org/10.3389/fimmu.2021.698565.
45. Yu PJ, Zhou M, Liu Y, Du J. Senescent T cells in Age-Related diseases. Aging Disease. 2025;16(1):321–44. https://doi.org/10.14336/AD.2024.0219.
46. Sakuishi K, Apetoh L, Sullivan JM, Blazar BR, Kuchroo VK, Anderson AC. Targeting Tim-3 and PD-1 pathways to reverse T cell exhaustion and restore anti-tumor immunity. J Exp Med. 2010;207(10):2187–94. https://doi.org/10.1084/jem.20100643.
47. Patrick M, Weng N. ping. Expression and regulation of telomerase in human T cell differentiation, activation, aging and diseases. Cell Immunol. 2019;345:103989. https://doi.org/10.1016/j.cellimm.2019.103989
48. Schumacher B, Pothof J, Vijg J, Hoeijmakers JHJ. The central role of DNA damage in the ageing process. Nature. 2021;592(7856):695. https://doi.org/10.1038/S41586-021-03307-7.
49. Saul D, Kosinsky RL, Atkinson EJ, et al. A new gene set identifies senescent cells and predicts senescence-associated pathways across tissues. Nat Commun. 2022;13(1). https://doi.org/10.1038/s41467-022-32552-1.
50. Tacutu R, Thornton D, Johnson E, et al. Human ageing genomic resources: new and updated databases. Nucleic Acids Res. 2018;46(D1):D1083–90. https://doi.org/10.1093/nar/gkx1042.
51. Ko A, Han SY, Choi CH, et al. Oncogene-induced senescence mediated by c-Myc requires USP10 dependent deubiquitination and stabilization of p14ARF. Cell Death Differ. 2018;25(6):1050–62. https://doi.org/10.1038/S41418-018-0072-0.
52. Schuster SJ, Svoboda J, Chong EA, et al. Chimeric antigen receptor T cells in refractory B-Cell lymphomas. N Engl J Med. 2017;377(26):2545–54. https://doi.org/10.1056/NEJMOA1708566/SUPPL_FILE/NEJMOA1708566_DISCLOSURES.PDF.
53. Finney OC, Brakke H, Rawlings-Rhea S, et al. CD19 CAR T cell product and disease attributes predict leukemia remission durability. J Clin Invest. 2019;129(5):2123–32. https://doi.org/10.1172/JCI125423.
54. Deng Q, Han G, Puebla-Osorio N, et al. Characteristics of anti-CD19 CAR T cell infusion products associated with efficacy and toxicity in patients with large B cell lymphomas. Nat Med. 2020;26(12):1878–87. https://doi.org/10.1038/s41591-020-1061-7.
55. Chong EA, Alanio C, Svoboda J, et al. Pembrolizumab for B-cell lymphomas relapsing after or refractory to CD19-directed CAR T-cell therapy. Blood. 2022;139(7):1026–38. https://doi.org/10.1182/BLOOD.2021012634.
56. Thurm C, Schraven B, Kahlfuss S. ABC transporters in T Cell-Mediated physiological and pathological immune responses. Int J Mol Sci. 2021;22(17). https://doi.org/10.3390/IJMS22179186.
57. Kraus ZJ, Haring JS, Bishop GA. TNF receptor-associated factor 5 is required for optimal T cell expansion and survival in response to infection. J Immunol (Baltimore Md: 1950). 2008;181(11):7800–9. https://doi.org/10.4049/JIMMUNOL.181.11.7800.
58. Bromley SK, Akbaba H, Mani V, et al. CD49a regulates cutaneous resident memory CD8 + T cell persistence and response. Cell Rep. 2020;32(9):108085. https://doi.org/10.1016/J.CELREP.2020.108085.
59. Wild CA, Bergmann C, Fritz G, et al. HMGB1 conveys immunosuppressive characteristics on regulatory and conventional T cells. Int Immunol. 2012;24(8):485–94. https://doi.org/10.1093/INTIMM/DXS051.
60. Bandala-Sanchez E, Bediaga NG, Goddard-Borger ED, et al. CD52 glycan binds the proinflammatory B box of HMGB1 to engage the Siglec-10 receptor and suppress human T cell function. Proc Natl Acad Sci USA. 2018;115(30):7783–8. https://doi.org/10.1073/PNAS.1722056115/-/DCSUPPLEMENTAL.
61. Sofiadis K, Josipovic N, Nikolic M, et al. HMGB1 coordinates SASP-related chromatin folding and RNA homeostasis on the path to senescence. Mol Syst Biol. 2021;17(6). https://doi.org/10.15252/MSB.20209760.
62. Lee JJ, Park IH, Rhee WJ, Kim HS, Shin JS. HMGB1 modulates the balance between senescence and apoptosis in response to genotoxic stress. FASEB Journal: Official Publication Federation Am Soc Experimental Biology. 2019;33(10):10942–53. https://doi.org/10.1096/FJ.201900288R.
63. Costa TDF, Zhuang T, Lorent J, et al. PAK4 suppresses RELB to prevent senescence-like growth arrest in breast cancer. Nat Commun. 2019;10(1). https://doi.org/10.1038/S41467-019-11510-4.
64. Dimri GP, Itahana K, Acosta M, Campisi J. Regulation of a senescence checkpoint response by the E2F1 transcription factor and p14(ARF) tumor suppressor. Mol Cell Biol. 2000;20(1):273–85. https://doi.org/10.1128/MCB.20.1.273-285.2000.
65. Pieren DKJ, Smits NAM, Postel RJ, et al. Co-Expression of TIGIT and helios marks immunosenescent CD8 + T cells during aging. Front Immunol. 2022;13. https://doi.org/10.3389/FIMMU.2022.833531.
66. van der List ACJ, Litjens NHR, Klepper M, Betjes MGH. Expression of senescence marker TIGIT identifies polyfunctional Donor-Reactive CD4 + T cells preferentially lost after kidney transplantation. Front Immunol. 2021;12. https://doi.org/10.3389/FIMMU.2021.656846.
67. Takahashi A, Imai Y, Yamakoshi K, et al. DNA damage signaling triggers degradation of histone methyltransferases through APC/C(Cdh1) in senescent cells. Mol Cell. 2012;45(1):123–31. https://doi.org/10.1016/J.MOLCEL.2011.10.018.
68. Kong W, Dimitri A, Wang W, et al. BET bromodomain protein inhibition reverses chimeric antigen receptor extinction and reinvigorates exhausted T cells in chronic lymphocytic leukemia. J Clin Invest. 2021;131(16). https://doi.org/10.1172/JCI145459.
69. Selli ME, Landmann JH, Terekhova M, et al. Costimulatory domains direct distinct fates of CAR-driven T-cell dysfunction. Blood. 2023;141(26):3153–65. https://doi.org/10.1182/blood.2023020100.
70. Amente S, Zhang J, Lavadera ML, Lania L, Avvedimento EV, Majello B. Myc and PI3K/AKT signaling cooperatively repress FOXO3a-dependent PUMA and GADD45a gene expression. Nucleic Acids Res. 2011;39(22):9498–507. https://doi.org/10.1093/nar/gkr638.

71. Kawalekar OU, O'Connor RS, Fraietta JA, et al. Distinct signaling of coreceptors regulates specific metabolism pathways and impacts memory development in CAR T cells. Immunity. 2016;44(2):380–90. https://doi.org/10.1016/j.immuni.2016.01.021.
72. Morrish F, Hockenbery D. MYC and mitochondrial biogenesis. Cold Spring Harb Perspect Med. 2014;4(5):a014225. https://doi.org/10.1101/cshperspect.a014225.

Publisher's note